Journal of Power Sources 272 (2014) 672–680

Contents lists available at ScienceDirect

Journal of Power Sources

journal homepage: www.elsevier.com/locate/jpowsour

Thermoelectric power enhancement by way of flow impedance for fixed thermal input conditions

Calil Amaral [a], Caio Brandão [b], Éric V. Sempels [c], Frédéric J. Lesage [d, e, *]

[a] Universidade Federal de Uberlândia, 2121 Av. João Naves de Ávila, Uberlândia 38.408-290, Brazil
[b] Universidade Federal da Paraíba, Cidade Universitária, CEP: 58051-900, João Pessoa, PB, Brazil
[c] École Polytechnique de Montréal, 2900 Boulevard Edouard-Montpetit, Montréal, Canada H3T 1J4
[d] Cégep de l'Outaouais, 333 boul. de la Cité-des-Jeunes, Gatineau, Canada J8Y 6M4
[e] Département d'informatique et d'ingénierie, Université du Québec en Outaouais, 101 rue Saint-9 Jean-Bosco, Gatineau, Canada J8Y 3G5

HIGHLIGHTS

- Flow channel impedance enhances thermoelectric power generation.
- Pumping penalty is offset by electric gain up to a threshold flow rate.
- Net thermoelectric power is measured relative to flow impeding panel density.
- Test cases include constant thermal input conditions for varying flow rates.

ARTICLE INFO

Article history:
Received 11 November 2013
Received in revised form
14 August 2014
Accepted 2 September 2014
Available online 16 September 2014

Keywords:
Thermal enhancement
Flow impedance
Thermoelectric
Power enhancement
Pumping penalty

ABSTRACT

Liquid-to-liquid thermoelectric generators are now being considered for the purpose of converting low cost heat to electricity for local energy uses. The importance in investigating their system efficiency lies in the fact that the generator's purpose is to maintain a heat source and a heat sink for its embedded thermoelectric modules. Of particular importance is the generator's ability to maintain an asymmetric thermal field across its embedded modules since this mechanism partially dictates the devices' thermal to electric conversion efficiency. Indeed, since the modules' semiconductor materials' ability to generate an electromotive force is dependent on the quality of the thermal dipole across the material, gains in thermoelectric generator energy conversion efficiency are made possible with thermal system management. In an effort to improve the system conversion efficiency of a liquid-to-liquid thermoelectric generator (TEG), the present work builds upon recent advancements in TEG inner pipe flow optimisation by investigating the thermoelectric power enhancement brought upon by flow impeding panel inserts in a thermoelectric generator's flow channels for fixed thermal input conditions and with respect to varying insert panel densities. The pumping penalty associated with the flow impedance is measured in order to present and to discuss the net thermoelectric power enhancement.

© 2014 Elsevier B.V. All rights reserved.

1. Introduction

Low-cost discarded heat is common place in domestic and industrial processes. Examples range from discarded stove heat to industrial cooling towers. In some processes excess heat is inconsequential and is expelled simply for lack of other uses and in other cases heat evacuation is necessary since it is damaging to operating equipment or hazardous to worker safety. Such residual low grade thermal energy is regarded as an inexpensive under-exploited source of energy and for this reason its conversion to electricity by way of the thermoelectric effect is ever more investigated. Furthermore, due to the fact that by-product heat is present in a wide range of processes, the ability to effectively convert its intrinsic thermal energy to electricity would serve a wide range of local energy needs.

To this end, studies investigating thermoelectric power production focus on improving a thermoelectric material's ability to generate an electromotive force from the asymmetric thermal field in which it is immersed or on the management of the thermal

* Corresponding author. Département d'informatique et d'ingénierie, Université du Québec en Outaouais, 101 rue Saint-9 Jean-Bosco, Gatineau, Canada J8Y 3G5. Tel.: +1 819 595 3900; fax: +1 819 773 1638.
E-mail addresses: Frederic.Lesage@uqo.ca, frederic.j.lesage@gmail.com (F.J. Lesage).

http://dx.doi.org/10.1016/j.jpowsour.2014.09.003
0378-7753/© 2014 Elsevier B.V. All rights reserved.

Nomenclature

c_p	specific heat at constant pressure, J kg^{-1}·K
D_p	linear panel density, panels/m
n	number of channels
p	pressure, PSI
P	power, W
P^*	P_i/P_o
P^+	net power enhancement
q	heat transfer rate, W
T	temperature, K
TEG	thermoelectric generator
TEM	thermoelectric module
$\dot{V}$	volumetric flow rate, m^3/s
$\Delta\dot{W}$	pumping penalty, W

Greek letters

α	seebeck coefficient, V/K
ρ	fluid density, kg m^{-3}

Subscripts

C	cold side
ch	channel
H	hot side
i	flow with inserts
in	inlet
o	flow without inserts
out	outlet

system maintaining the heat source and the heat sink. Indeed, the properties of thermoelectric materials have been investigated by the likes of André et al. [1] and Poudeu et al. [2] in an effort to design alloy combinations which better mobilise the semiconductor's charge carriers in an electric circuit. It has also been shown in studies such as those of Min and Rowe [3], Ebling et al. [4], Hadjistassou et al. [5] and others [e.g., Ref. [6]] that material thermoelectric conversion efficiency can be improved through geometric design and by segmenting thermoelectric elements into combined pellets which enhance charge carrier concentration while lessening heat conduction. The interaction between the thermal field and the electrical potential have been investigated and modelled by Wang et al. [7,8] and applied to practical applications such as battery recharging [e.g., Ref. [9]], pulse laser cooling [10] and solar thermoelectric recovery [e.g., Ref. [11]] among others. Furthermore, recent advancements into flexible thermoelectric modules [e.g., Ref. [12]] provide a trajectory to applications using previously unexploited heat sources. In general, these studies into thermoelectric material characteristics seek to maximise the charge carrier's transported entropy relative to the material's heat conduction capacity for target heat sources and target heat sinks. The results of these efforts have shown that waste-heat applications below 450 K are most promising when using thermoelectric modules which combine the alloys bismuth (Be) and tellurium (Te). Indeed, devices in which Bi_2Te_3 semiconductor pellets are assembled thermally in parallel and electrically in series have been identified by Karabetoglu et al. [13] as the most promising commercially available thermoelectric modules for low grade heat applications ranging in temperatures between 273 and 473 K which corresponds to typical waste-heat processes [14]. A detailed description of the thermoelectric characteristic of an individual Bi_2Te_3 pellet leg is provided by Favarel et al. [15]. As shown by Meng et al. [16], the thermal energy to electrical power conversion may also be enhanced by improving the heat transfer from the heat source to the modules and from the modules to the heat sink thereby increasing the thermal potential across the modules which drives the electromotive force responsible for increasing charge carrier concentration. Such gains are significant since the use of the current state-of-the-art in thermoelectric generator technology is not wide spread due to a lack of cost effectiveness. For this reason, investigations into practical applications of thermoelectric power production focus on thermal system management in order to maintain and optimise a potentially asymmetric thermal field. Such works vary with respect to the intended heat source and the available heat sink. Specific examples include generator designs in which thermoelectric modules are embedded between alternating cold and hot plates containing fluid flow channels [e.g., Refs. [17–19]]. In these studies, optimal thermal system management including flow characteristics and module placement for optimal thermoelectric power output is experimentally and numerically investigated [e.g., Refs. [20–23]]. Target applications include residual heat in flow channels resulting from industrial heat exchangers and vehicle exhaust [e.g., Refs. [24–32]].

In the present work, it is shown that for constant thermal input conditions the power output of a thermoelectric liquid-to-liquid generator increases with increasing flow rate. It is also shown to increase with increasing flow impeding panel density of a specified geometric form. The pumping penalty relative to an absence in flow impeding geometries is measured in order to evaluate the flow rate range in which thermoelectric power enhancement due to flow impedance is positive. Furthermore, flow simulations are used to discuss the experimentally measured thermal transport results.

2. Experimental set up

2.1. Thermoelectric power

The objective of the test apparatus is to effectively supply and remove heat from a series of embedded thermoelectric modules containing the material Bismuth Telluride (Bi_2Te_3). The desired effect is to create a thermal potential across the materials which generates an electromotive force mobilizing charge carriers. The thermoelectric materials are doped either positively or negatively in order to favour a positive charge carrier transport or a negative charge carrier transport. The target heat source and target heat sink used to maintain the thermal dipole are hot and cold fluid flow respectively. The general concept is illustrated in Fig. 1 showing an idealized thermocouple cycling a current through a positive charge carrier thermo-pellet leg and a negative thermo-pellet leg which are electrically connected at the extrema of an idealized thermal dipole.

2.2. Thermoelectric generator (TEG)

The thermal potential driving the electromotive force is facilitated by a thermoelectric generator (TEG) consisting of two sets of twenty commercially available thermoelectric modules TEG2-07025HT-SS connected electrically in series with embedded n-type and p-type Bi_2Te_3 thermoelectric pellet legs. Each module measures 40 mm × 40 mm × 4.3 mm the average cross section of the semiconductor pellets within each module is 5.7 mm^2 and their average length is 1.33 mm. These elements are set in ten rows of twelve and two rows of ten within the module in which the last two rows are shorter to yield space for the electrical connections. A comprehensive characterisation of Bi_2Te_3 thermoelectric properties

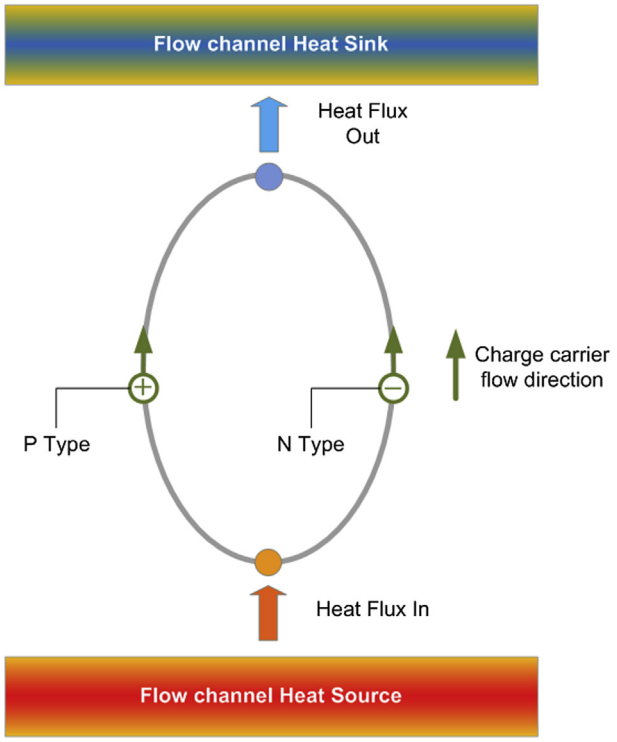

Fig. 1. Thermoelectric power generation from a thermal dipole maintained by a flow channel heat source and a flow channel heat sink.

including its Seebeck coefficient and Figure-of-merit are detailed in Favaral et al. [15]. The modules are placed on either side of parallel hot fluid flow channels which are enclosed by two layers of two cold fluid flow channels. A schematic representation of the aluminium encased generator and its electrical circuit are provided in Fig. 2.

The generator has a total of six flow pipes in which two channel hot water through its central longitudinal axis. In addition, two sets of two flow pipes channel cold water through its upper and lower portions. Each internal pipe diameter is 9.29 mm and the hot and cold are set up in a counter-flow configuration. This is noteworthy since a thermoelectric generator design can attempt to increase its number of thermoelectric modules in contact with its heat source and heat sink by stacking the flow channels [e.g., Ref. [18]], however this necessarily leads to sections in which the hot and cold channels flow in parallel. In the present study, a counter flow configuration has been purposefully commissioned in order to produce the most homogeneous thermal profile the length of the generator. Indeed, in parallel flow, the thermal transport between the cold and hot fluid channels will result in a temperature difference that differs more greatly between the inlet and outlet values. In the contour flow configuration, the thermal energy exchange experienced at the hot fluid inlet (corresponding to the cold fluid outlet) more closely resembles the thermal energy exchange at the hot fluid outlet (corresponding to the cold fluid inlet). In its entirety, the aluminium encased generator containing the flow pipes and the thermoelectric modules measures 472.0 mm × 90.0 mm × 60.0 mm.

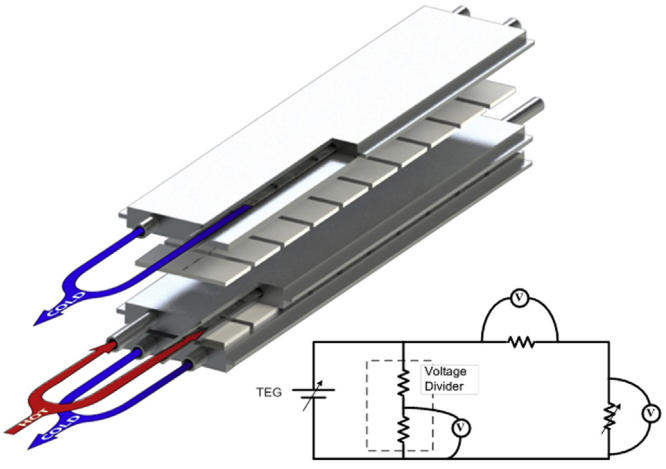

Fig. 2. Thermoelectric liquid-to-liquid generator assembly.

2.3. Experimental test-stand

An experimental test-stand is built in order to control the thermal input conditions and the inlet flow rates of the TEG. Specifically, a purpose built work bench supports the generator to which a hot water circuit and a cold water circuit is connected. A Styrofoam thermal insulation covers the TEG and the entire work bench with the water circuits and the TEG are enclosed in a Plexiglass casing to protect from possible hot water hazards. The hot water circuit inlet temperature and inlet flow rate are controlled using a MicroTherm CMX Series Temperature Control System. This effectively combines a pumping and heating system resulting in a controlled flow rate and temperature for the TEG's heat source.

The hot and cold inlet temperatures are measured using Type T thermocouples relaying readings to an Omega RDXL4SD 4-Channel Datalogger Thermometer to an accuracy of ±(0.4% + 0.5 °C). The flow rate of the hot fluid flow circuit and the cold fluid flow circuit are each measured with separate OMEGA – MR Flow Transmitters relaying sensor readings to the interface ScienceWorkshop 750 and recorded using DataStudio software. The voltage and the electric current are also measured and recorded using the ScienceWorkshop 750 and DataStudio data acquisition package. In this way, the electric power output of the generator is computed. The impedance of the electrical load resistance is measured to an accuracy of 20.0 ± 0.5% Ω using a Metex M-3800 Digital Multimeter.

Furthermore, due to the flow impedance of the flow turbulating inserts of the present study, care is taken to accurately measure the pressure drop across the flow channels resulting from the presence of the inserts. In this way, the added work due to the pressure drop resulting from the flow impeding inserts, referred to as the pumping penalty in the present document, can be calculated in the following way.

$$\Delta\dot{W} = n(\Delta p_i - \Delta p_o)\dot{V} \quad (1)$$

in which n is the number of pipes, Δp_i is the pressure drop along a flow channel with a flow impeding insert, Δp_o is the pressure drop along a flow channel without a flow impeding insert and $\dot{V}$ is the volumetric fluid flow rate. To this end, Omega DPG1001B-100G High-Accuracy Digital Pressure Gauges are placed at the cold fluid circuit entry and exit and at the hot fluid circuit entry and exit from the TEG. These pressure valves have a resolution of 0.1psi with an accuracy of ±0.10%.

A full schematic representation of the hot and cold fluid flow circuits is presented in Fig. 3.

In an effort to measure the electric power enhancement that is a result of the flow impedance with respect to flow rate for fixed

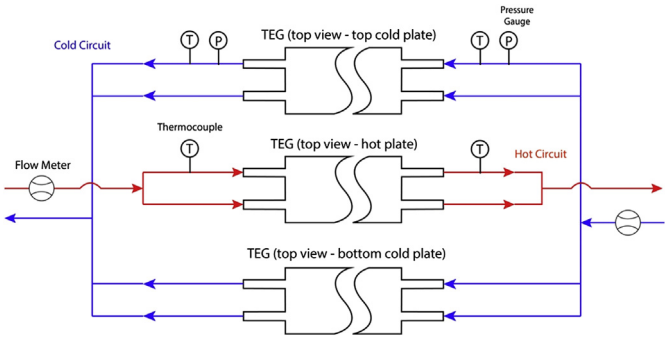

Fig. 3. Schematic representation of fluid flow circuits including the positioning of the pressure gauges, thermocouples and flow metres relative to the thermoelectric generator (TEG).

thermal input conditions, the temperature difference at the hot and cold inlets is maintained at $\overline{\Delta T_{in}} = 70.6 \pm 1.0^{\circ}C$.

2.4. Flow impeding inserts

In an effort to measure the thermoelectric power enhancement relative to the density of the alternating panels of the flow impeding inserts, a custom made steel punch and die mold is commissioned in order to manufacture flow impeding inserts of varying panel density but otherwise equivalent. These inserts are made of galvanized steel strips having a cross section of 0.50 mm × 8.66 mm and are long enough to run the length of the generator. They are defined in this document by the density of the panels which range from 0 to 125 panels/m. The punch and die and an example of a resulting flow impeding insert are illustrated in Fig. 4.

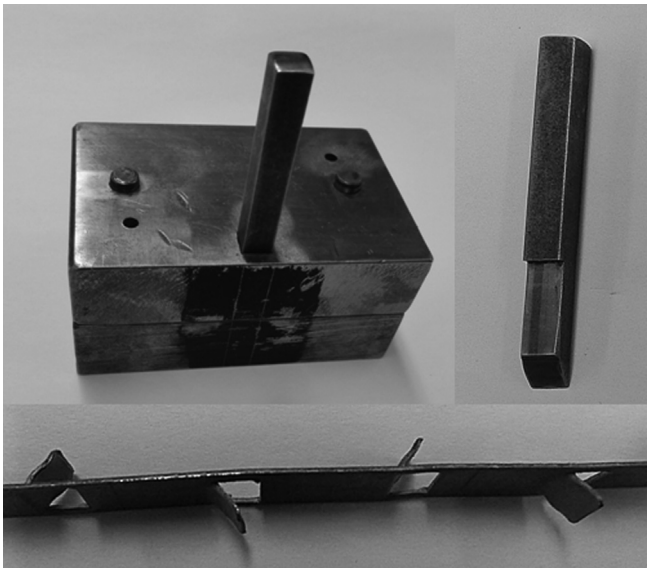

Fig. 4. (Top) Steel punch and die mold used to manufacture flow impeding inserts from galvanized steel strips; (Bottom) Flow impeding insert with a panel density of 62.5 panels/m.

3. Results and discussion

3.1. Flow and insert performance comparison

The thermoelectric power output is tested for working conditions in which the thermal input is such that the temperature difference between the hot and cold flows upon entry to the generator is 70.6 ± 1.0 °C. Furthermore, TEG power output during operation without inserts and with inserts is measured over a range of flow rates. The two varying parameters are therefore the flow impeding insert panel density (D_p) and the fluid flow rate ($\dot{V}$). A system efficiency analysis of the present setup is available in Amaral et al. [33]. During TEG operation all flow channels operate at the same flow rate and all channels are fitted with inserts of the same geometry and panel density. The results illustrated in Fig. 5 show the measured electric power generated by the TEG with respect to insert panel density and fluid flow rate. The results show that electric power output increases with increasing flow rate and with increasing panel density.

The increase in measured electric power with respect to an increase in flow rate observed in Fig. 5 is attributed to a more homogenous longitudinal thermal field within the generator. More specifically, at the upper flow rate limit, the inlet and outlet temperature of the water converge which implies that all of the embedded thermoelectric modules are subject to a more homogenous temperature difference the length of the TEG thereby producing a maximum power output. As an illustrative example, water entering the channel at 80 L min^{-1}channel^{-1} for the given channel geometry of the TEG has 0.03 s to exchange heat with the generator's thermoelectric materials rather than 2.4 s at 1 L min^{-1}channel^{-1}. At low volumetric flow rates, the flow experiences a relatively high temperature variation from inlet to outlet within the generator which implies that the first and last TEMs in the longitudinal direction work under lower temperature difference conditions thereby making the TEG device operate below its maximum capacity. Fig. 6 illustrates the comparison made using values obtained for two different flow rates with flow impeding inserts of panel density 31.2 panels/m. It illustrates that a greater temperature difference is maintained at higher flow rates than lower flow rates for equal thermal input conditions.

The power increase due to the increase in insert panel density is discussed in a forth coming section which evaluates the temperature drop across each channel with respect to insert panel density.

3.2. Thermoelectric power enhancement

In order to evaluate and compare the performance of different geometries, the power enhancement is calculated using the non-dimensional index P^* which represents the ratio of TEG power output operating with inserts to power output operating with unobstructed flow channels. It is defined as.

$$P^* = \frac{P_i}{P_o} \tag{2}$$

in which P_i is the enhanced thermoelectric power with inserts and P_o is the measured power without inserts.

The results are presented in Fig. 7 in which rational functions are fit to the curves representing the thermoelectric power enhancement of each insert with respect to flow rate. The thermal input conditions are maintained at $\overline{\Delta T_{in}} = 70.6 \pm 1.0$ °C. The horizontal line for which P^* attains unity represents the limit region in which the power enhancement is nil.

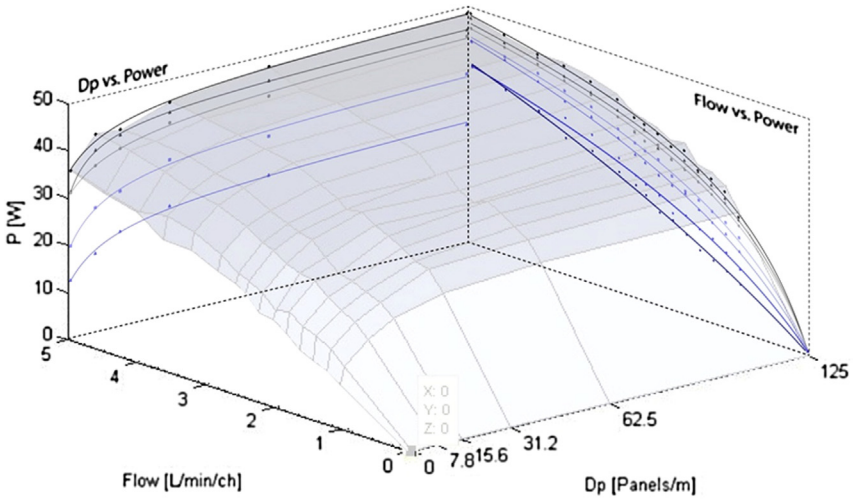

Fig. 5. Measured electric power output with respect to flow rate and flow impeding panel density.

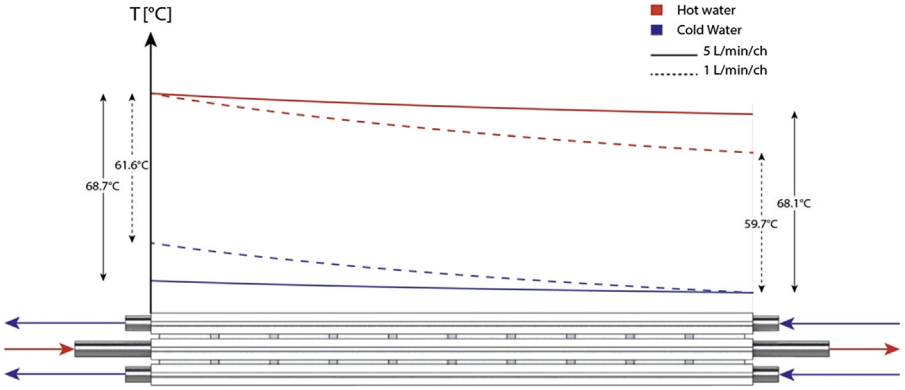

Fig. 6. Temperature difference the length of the TEG for equal thermal input conditions at flow rates of 5 L min^{-1} ch^{-1} and 1 L min^{-1} ch^{-1} with flow impeding inserts having a panel density of 31.2 panels/m.

Consistent with previous results, Fig. 7 illustrates that the thermoelectric power enhancement due to flow impeding inserts increases with increasing panel density. Fig. 7 does reveal however that this enhancement diminishes in relative importance for increasing flow rate. This implies that a threshold flow rate exists in which the pumping power required to increase flow rate is not offset by the gain in thermoelectric power. This is investigated in a forthcoming section in which the thermoelectric enhancement less the pumping penalty is measured.

3.3. Thermal enhancement

The power enhancement illustrated in Fig. 7 is attributed to two principal factors. The first is the more homogenous thermal field at higher flow rates as previously illustrated in Fig. 6. The second is an

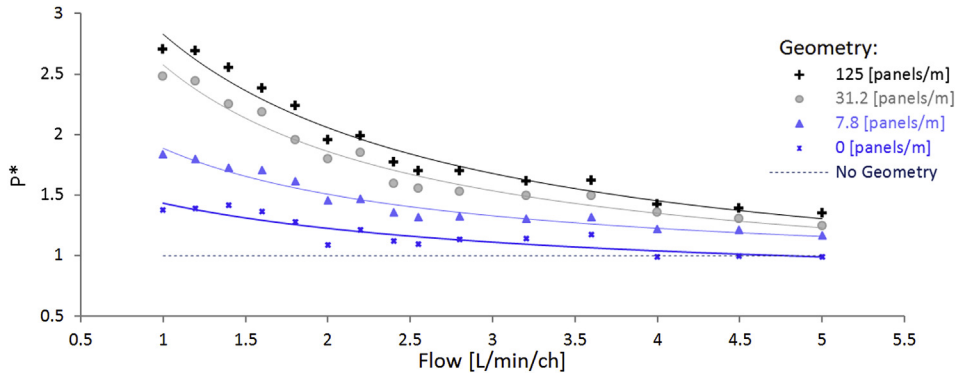

Fig. 7. Thermoelectric Power Enhancement with respect to panel density.

alteration in the mean velocity vectors due to the flow impeding inserts. More specifically, radial components in the mean velocity vectors become more pronounced due to the altered flow patterns. As a result, near the channel inner walls the thermal boundary layer is reduced thereby improving the thermal transport to the adjacent modules. Indeed, [31,33] showed that impeding inserts with a panel configuration create secondary flows in radial directions thereby increasing the radial temperature gradient component. This increased local alignment of the temperature gradient with the velocity profile is known as the field synergy principal and is responsible for a thermal transport enhancement [e.g., Refs. [34–37]]. In the context of a liquid-to-liquid thermoelectric generator, the field synergy effect serves to increase the heat flux at the periphery of the hot and cold flow channels. This in turn improves the generator's embedded modules' heat source and heat since thereby increasing the temperature differential across the embedded thermoelectric modules.

In the present study, the longitudinal inner pipe flow is altered using impeding geometries. The altered velocity field is shown through numerical simulations to increase the radial components of the velocity vectors. Since the heat flux is principally at the channel walls, the thermal field has primarily radial components. This implies that the flow impeding inserts are responsible for increasing the local alignment of the velocity field with the temperature gradient thereby enhancing the thermal transport. The rate of heat transfer q out of the hot flow channel is calculated from the simplified steady-flow thermal energy equation.

$$q = \dot{V}\rho c_{\mathrm{p}}(T_{\mathrm{out}} - T_{\mathrm{in}}) \tag{3}$$

in which ρ and c_p are the density and the specific heat respectively of the working fluid.

Since in the present study the test cases are measured at a fixed flow rate for fixed thermal input conditions, the temperature drop the length of the hot flow channel is measured in order to quantify the heat transfer capabilities per flow rate per insert geometry. The results illustrated in Fig. 8 show that at the low end of the flow rates, below 2.5 L min^{-1}channel^{-1}, the heat transfer is enhanced when impeding the flow with high panel density inserts. The results also show that for higher flow rates in the range of 3–5 L min^{-1}channel^{-1}, the heat transfer decreases with respect to insert panel density. The thermal transport mechanism responsible for the differences in temperature drop are discussed using the forthcoming numerical simulations of the inner pipe flow.

3.4. Flow simulations

The difference in thermal transport behaviour with respect to insert panel density is best explained with the use of inner flow simulations describing the velocity field for a cross sectional portion of the flow channel. To this end, the flow is simulated using SolidWorks Flow Simulation CFD software's integrated turbulent intensity and length model. The simulations are run for an inlet flow rate of 1 L min^{-1} and again for 5 L min^{-1} in a channel of equivalent geometry to that of the test device with an outlet condition of atmospheric pressure. The simulations are repeated for conditions in which there are no obstructions to the flow within the flow channel and again for which a flow impeding geometry is inserted with a panel density of 125 panels/m. Each simulation is run over 160 iterations and yields a flow velocity gradient along the channel.

The results of the inner flow simulations are shown in Figs. 9–12 and serve to explain the difference in heat transfer behaviour at different flow rates and different panel densities.

The inner channel flow simulations illustrated in Figs. 9–12 show that:

1. For the test case in which the velocity field has a 1 L min^{-1} inlet flow rate, the velocity boundary layer adjacent to the inner channel periphery is reduced by a factor of approximately 4.80 when flow is impeded by the panel inserts. This implies that in the presence of the flow impeding inserts, there is a greater thermal gradient perpendicular to the flow thereby enhancing the heat transfer at the inner channel walls.
   It is also important to note that despite greatly reducing the velocity boundary layer, the flow field adjacent to the boundary layer is only increased by a factor of 1.5. Therefore, for the low inlet flow rate of 1 L min^{-1}, the temperature drop increased in the presence of the flow impeding panels is attributed to a significant decrease in velocity boundary layer.
2. For the test case in which the velocity field has a 5 L min^{-1} inlet flow rate, the panel inserts do not significantly decrease the velocity boundary layer. This is due to the fact that at this higher flow rate, a more homogenous velocity field is generated resulting in a central axis flow approaching the periphery of the flow channel more closely than at lower flow rates. Similar to the lower flow rate simulation, the presence of the flow impeding inserts creates annular flow altering the velocity boundary layer and the mean velocity adjacent to the boundary layer. However, for the higher inlet flow rate of 5 L min^{-1}, the velocity boundary layer is only reduced by a factor of 1.45 in the

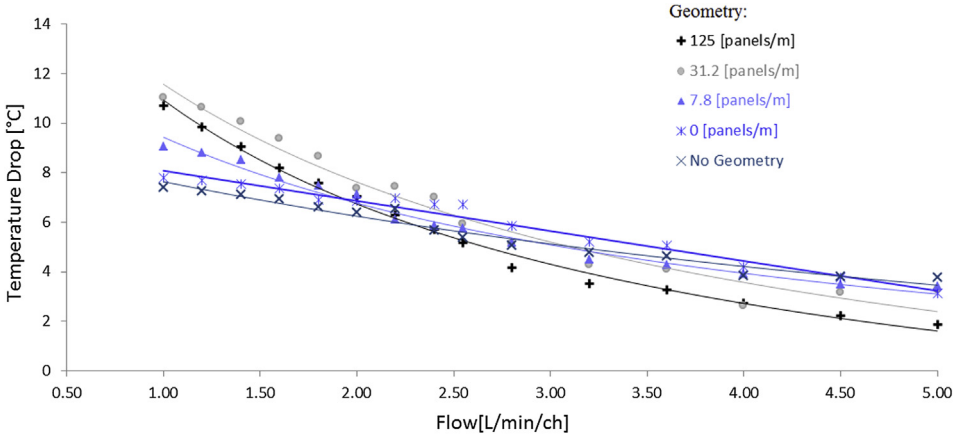

Fig. 8. Temperature drop in the hot fluid flow channel.

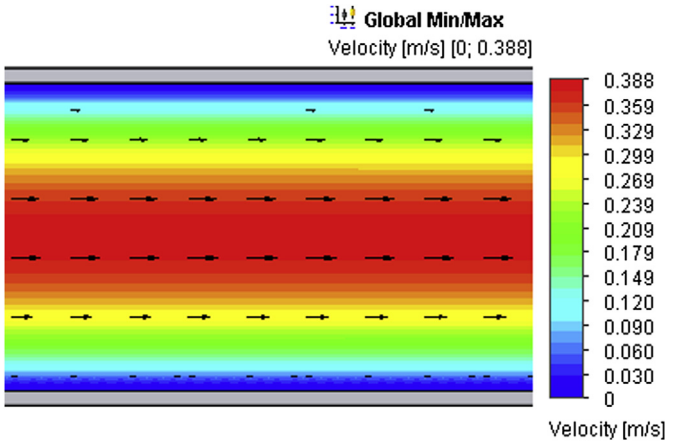

Fig. 9. Channel flow velocity profile for a 1 L min^{-1} inlet flow rate without flow impeding inserts.

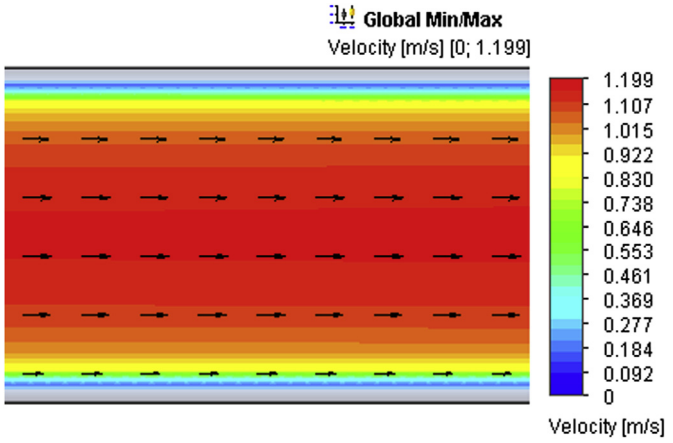

Fig. 10. Channel flow velocity profile for a 5 L min^{-1} inlet flow rate without flow impeding inserts.

presence of the flow impeding insert relative to an absence of inserts while the mean velocity adjacent to the boundary layer is increased by a factor of 6.1.

The decrease in the temperature drop experimentally measured at 5 L min^{-1} in the presence of the flow impeding geometries is

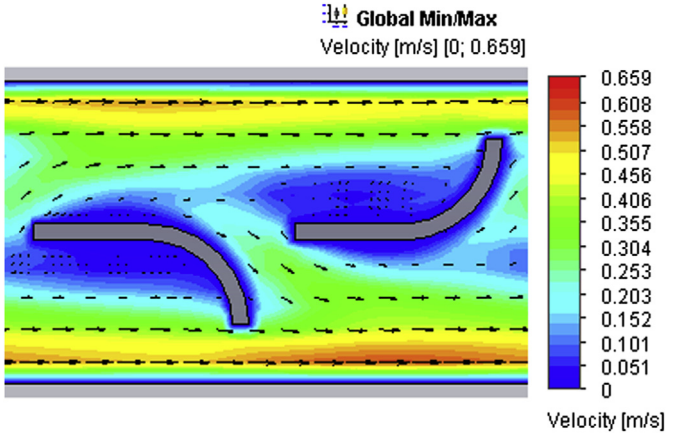

Fig. 11. Channel flow velocity profile for a 1 L min^{-1} inlet flow rate with flow impeding inserts having a panel density of 125 panels/m.

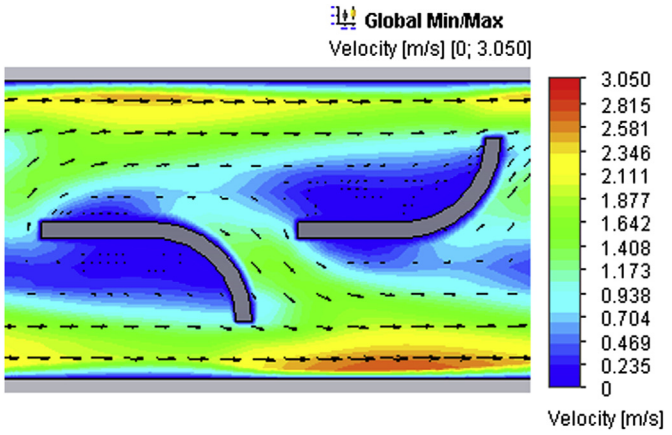

Fig. 12. Channel flow velocity profile for a 5 L min^{-1} inlet flow rate with flow impeding inserts having a panel density of 125 panels/m.

therefore attributed to the high flow rate adjacent to the velocity boundary layer which offsets the thermal transport benefits gained by the reduced boundary layer thickness. Indeed, due to the field synergy principle, an increase in mean velocity in the longitudinal direction results in a decrease in the radial thermal transport.

It is observed in Fig. 8 that the temperature drop at 1 L min^{-1} for a panel density of 125 panels/m is less than that for 31.25 panels/m. This is explained through an analysis of the temperature drop with respect to the panel density parameter D_p and the field synergy principle. In examining the flow characteristics associated with the lower panel density limit, Fig. 9 shows that the insert with D_p equal to zero panels/m favours a longitudinal mean flow direction rather than radial thereby minimising the field synergy effect. Conversely, Fig. 13 presents the simulated velocity profile for the upper panel density limit. The geometric characteristics of the panel inserts and the flow pipes yield an upper panel density limit of 1000 panels/m for which each panel is in contact with its neighbouring panel.

The results of Fig. 13 show that the radial velocity components are minimised for the upper panel density limit (1000 panels/m) as for the lower panel density limit (0 panels/m) since the panels effectively create a solid central obstruction. Specifically, in the case of Fig. 13, the flow is restricted to an annular flow in which the longitudinal mean velocity is greater than the input velocity. Consequently, the absence of the radial component of the velocity vectors for the upper and lower panel density limits implies that there exists a critical panel density between the lower and upper limits which maximises the thermal transport enhancement due to the field synergy principal. Indeed, it is shown in Fig. 8 that the panel density of 125 panels/m is beyond the critical threshold since it yields inferior temperature drops when compared with the 31 panels/m result.

It is important to note that despite a decrease in thermal transport in the presence of flow impeding inserts at the higher flow rates, as illustrated in Fig. 8, the thermoelectric power produced by the TEG increases with flow impeding geometries, albeit to a lesser extent than at the lower spectrum of the flow rates. This is a significant observation since the electric current is powered by the thermal potential created by the heat source and the heat sink and as such a decrease in thermal transport capabilities should entail a decrease in thermoelectric power. This is explained by the increase in mean velocity adjacent to the velocity boundary layer brought upon by the flow impeding geometries. Although, this increase in velocity impedes the thermal transport at the periphery of the flow channel, it also provides a more homogenous thermal

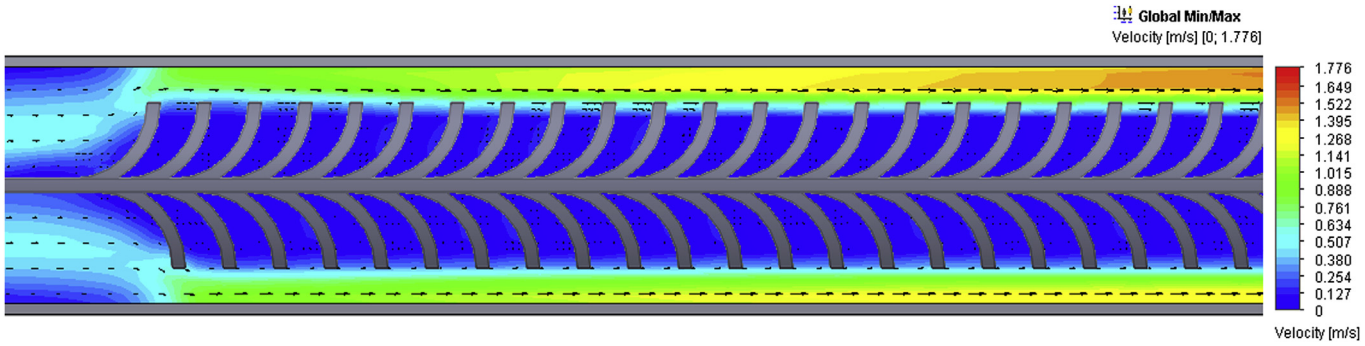

Fig. 13. Channel flow velocity profiles for a 1 L min^{-1} inlet flow rate with flow impeding inserts having a panel density of 1000 panels/m.

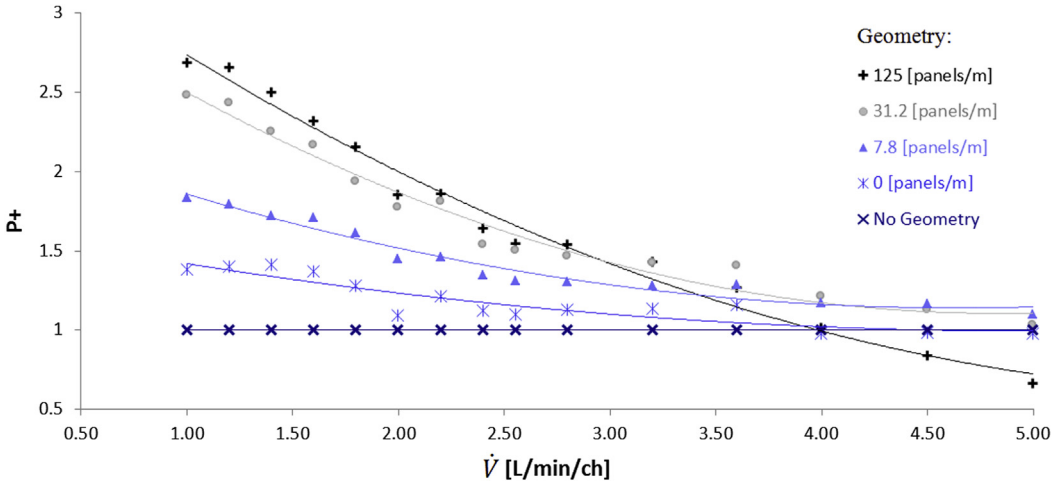

Fig. 14. Net thermoelectric power enhancement accounting for pumping penalty due to flow impeding inserts relative to flow with no inserts.

profile the length of the generator's flow channels to which it is sensitive, due to the counter-flow configuration, as previously discussed in Fig. 6. Therefore, the decrease in thermal transport capabilities due to the presence of the insert geometries at higher flow rates is offset by an increase in thermal profile homogeneity the length of the flow channel resulting in an increase in thermoelectric power generation.

3.5. Net thermoelectric power enhancement

The net thermoelectric power enhancement measures the power output with flow impeding inserts less the added work due to an increase in pressure drop relative to pipe flow in absence of any inserts. The net thermoelectric power enhancement P^+ is defined as.

$$P^+ = \frac{P_i - \Delta\dot{W}}{P_o}. \quad (4)$$

Fig. 14 presents the TEG's net power enhancement over varying flow rates. An important feature is that beyond a threshold flow rate, an increase in insert panel density results in a pumping penalty that is not offset by the power enhancement. In particular a P^+ of unity implies that there is no net gain or loss relative to power output without flow impeding inserts. The results show that for flow rates beyond 4 L min^{-1}channel^{-1}, the net power enhancement falls below unity during TEG operation with inserts of 125 panels/m, implying a loss relative to operation with no inserts. Conversely, for lower flow rates, TEG operation with insert panel density of 125 panels/m is measured to enhance the power gain by more than a factor of 2.5 relative to TEG operation without inserts.

The patterns observed in Fig. 14 suggest that there is an optimum insert panel density relative to flow rate for which maximum power output is obtained.

4. Conclusion

In the present work, the electric power output of a liquid-to-liquid thermoelectric generator is measured for fixed thermal input conditions over a range of flow rates. Each test case is repeated with a series of flow impeding panel inserts. The main thesis of this work is to evaluate the thermoelectric power gain due to the presence of flow impedance in the flow channels. This flow impedance is managed with flow impeding panel inserts which are identified by the density of their alternating panels. It is shown that the electric power output of the test liquid-to-liquid thermoelectric generator increases with increasing flow rate and with increasing insert panel density. Furthermore, flow simulations are performed in an effort to attribute the measured thermal transport mechanisms to flow field profiles.

In order to account for the pumping penalty due to the presence of the flow impeding geometries, the net thermoelectric enhancement is defined and measured. The results show that there exists an upper threshold flow rate in which the thermoelectric power gain brought upon by the flow impeding inserts no longer offsets the work due to their presence. Indeed, it is shown that, for

the thermal input conditions of the present study, an optimal flow impeding insert panel density exists for a given flow rate yielding a maximum net thermoelectric power output.

Acknowledgements

The authors gratefully thank the Fonds de recherche nature et technologie (FQRNT) grant 2015-CO-186489, the Brazilian Conselho Nacional de Pesquisa e Desenvolvimento Tecnológico (CNPq), and the Canadian Bureau for International Education (CBIE) for their generous support throughout this project. The authors also thank Rémi Pelletier for his exceptional technical expertise.

References

[1] C. André, D. Vasilevskiy, S. Turenne, R.A. Masut, J. Electron. Mater. 38 (2009) 1061–1067.
[2] P.F.P. Poudeu, A. Guéguen, C.-I. Wu, T. Hogan, M.G. Kanatzidis, Chem. Mater. 22 (2010) 1046–1053.
[3] G. Min, D.M. Rowe, J. Power Sources 38 (3) (1992) 253–259.
[4] D. Ebling, K. Bartholomé, M. Bartel, M. Jägle, J. Electron. Mater. 39 (2010) 1376–1380.
[5] C. Hadjistassou, E. Kyriakides, J. Georgiou, Energy Convers. Manag. 66 (2013) 165–172.
[6] A. Rezania, L.A. Rosendahl, H. Yin, J. Power Sources 255 (2014) 151–156.
[7] X.D. Wang, Y.X. Huang, C.H. Cheng, D. Ta-Wei Lin, C.H. Kang, Energy 47 (1) (2012) 488–497.
[8] X.D. Wang, Q.H. Wang, J.L. Xu, Energy 65 (2014) 419–429.
[9] C.E. Kinsella, S.M. O'Shaughnessy, M.J. Deasy, M. Duffy, A.J. Robinson, Appl. Energy 114 (2014) 80–90.
[10] L. Shen, H. Chen, F. Xiao, Y. Yang, S. Wang, Energy Convers. Manag. 80 (2014) 39–45.
[11] A.K. Trinh, I. González, L. Fournier, R. Pelletier, V.,J.C. Sandoval, F.J. Lesage, Appl. Therm. Eng. 70 (1) (2014) 675–686.
[12] J.H. We, S.J. Kim, B.J. Cho, Energy 73 (2014) 506–512.
[13] S. Karabetoglu, A. Sisman, Z. Faith Ozturk, T. Sahin, Energy Convers. Manag. 62 (2012) 47–50.
[14] D.M. Rowe, G. Min, J. Power Sources 73 (2) (1998) 193–198.
[15] C. Favarel, J.P. Bédécarrats, T. Kousksou, D. Champier, Energy 68 (2014) 104–116.
[16] J.H. Meng, X.X. Zhang, X.D. Wang, J. Power Sources 245 (2014) 262–269.
[17] H. Zhao, J. Yu, J. Power Sources 172 (2007) 428–434.
[18] X. Niu, J. Yu, S. Wang, J. Power Sources 188 (2009) 621–626.
[19] T. Kousksou, J.P. Bédécarrats, D. Champier, P. Pignolet, C. Brillet, J. Power Sources 196 (8) (2011) 4026–4032.
[20] X. Gou, H. Xiao, S. Yang, Appl. Energy 87 (2010) 3131–3136.
[21] S. Bélanger, L. Gosselin, Energy Convers. Manag. 52 (2012) 2911–2918.
[22] J.Y. Jang, Y.C. Tsai, Appl. Therm. Eng. 51 (1) (2013) 677–689.
[23] D.T. Crane, G.S. Jackson, Energy Convers. Manag. 45 (2004) 1565–1582.
[24] J.W. Stevens, Energy Convers. Manag. 42 (2001) 709–720.
[25] C. Yu, K.T. Chau, Energy Convers. Manag. 50 (2009) 1506–1512.
[26] E.W. Miller, T.J. Hendricks, R.B. Peterson, J. Electron. Mater. 38 (2009) 1206–1213.
[27] D. Dai, Y. Zhou, J. Liu, Renew. Energy 36 (2011) 3530–3536.
[28] N.R. Kristiansen, G.J. Snyder, H.K. Nielsen, L. Rosendahl, J. Electron. Mater. 41 (2012) 1024–1029.
[29] T.J. Hendricks, N.K. Karri, T.P. Hogan, C.J. Cauchy, J. Electron. Mater. 42 (7) (2013) 1725–1736.
[30] F.J. Lesage, N. Pagé-Potvin, Energy Convers. Manag. 66 (2013) 98–105.
[31] F.J. Lesage, E.V. Sempels, N. Lalande-Bertrand, Energy Convers. Manag. 75 (2013) 532–541.
[32] F. Meng, L. Chen, F. Sun, B. Yang, Energy 66 (2014) 965–972.
[33] C. Amaral, C. Brandão, É.V. Sempels, F.J. Lesage, Appl. Therm. Eng. 65 (1) (2014) 94–101.
[34] J.M. Wu, W.Q. Tao, Appl. Therm. Eng. 27 (14) (2007) 2609–2617.
[35] Y.P. Cheng, T.S. Lee, H.T. Low, Appl. Therm. Eng. 28 (14) (2008) 1826–1833.
[36] J. Li, H. Peng, X. Ling, Appl. Therm. Eng. 54 (1) (2013) 328–335.
[37] Y. Li, J. Wu, L. Zhang, L. Kou, Appl. Therm. Eng. 31 (14) (2011) 3078–3083.